Bioorganic & Medicinal Chemistry 18 (2010) 3413–3425

Contents lists available at ScienceDirect

Bioorganic & Medicinal Chemistry

journal homepage: www.elsevier.com/locate/bmc

1-(3-Deoxy-3-fluoro-β-D-glucopyranosyl) pyrimidine derivatives as inhibitors of glycogen phosphorylase b: Kinetic, crystallographic and modelling studies

Vicky G. Tsirkone [a], Evangelia Tsoukala [b], Christos Lamprakis [a], Stella Manta [b], Joseph M. Hayes [a], Vicky T. Skamnaki [a], Christina Drakou [a], Spyros E. Zographos [a], Dimitri Komiotis [b], Demetres D. Leonidas [b,*]

[a] Institute of Organic & Pharmaceutical Chemistry, National Hellenic Research Foundation, 48 Vas. Constantinou Avenue, 11635 Athens, Greece
[b] Department of Biochemistry and Biotechnology, University of Thessaly, 26 Ploutonos Str., 41221 Larissa, Greece

ARTICLE INFO

Article history:
Received 4 February 2010
Revised 26 March 2010
Accepted 1 April 2010
Available online 7 April 2010

Keywords:
Glycogen phosphorylase
Diabetes
X-ray crystallography
Structure-assisted inhibitor design
Glide docking
Quantum mechanics polarized ligand (QPLD) docking
Tautomers

ABSTRACT

Design of inhibitors of glycogen phosphorylase (GP) with pharmaceutical applications in improving glycaemic control in type 2 diabetes is a promising therapeutic strategy. The catalytic site of muscle glycogen phosphorylase b (GPb) has been probed with five deoxy-fluro-glucose derivatives. These inhibitors had fluorine instead of hydroxyl at the 3′ position of the glucose moiety and a variety of pyrimidine derivatives at the 1′ position. The best of this carbohydrate-based family of five inhibitors displays a K_i value of 46 μM. To elucidate the mechanism of inhibition for these compounds, the crystal structures of GPb in complex with each ligand were determined and refined to high resolution. The structures demonstrated that the inhibitors bind preferentially at the catalytic site and promote the less active T state conformation of the enzyme by making several favorable contacts with residues of the 280s loop. Fluorine is engaged in hydrogen bond interactions but does not improve glucose potency. The pyrimidine groups are located between residues 284–286 of the 280s loop, Ala383 of the 380s loop, and His341 of the β-pocket. These interactions appear important in stabilizing the inactive quaternary T state of the enzyme. As a follow up to recent computations performed on β-D-glucose pyrimidine derivatives, tautomeric forms of ligands **1–5** were considered as potential binding states. Using Glide-XP docking and QM/MM calculations, the ligands **2** and **5** are predicted to bind in different tautomeric states in their respective GPb complexes. Also, using α-D-glucose as a benchmark model, a series of substitutions for glucose –OH at the 3′ (equatorial) position were investigated for their potential to improve the binding affinity of glucose-based GPb catalytic site inhibitors. Glide-XP and quantum mechanics polarized ligand (QPLD-SP/XP) docking calculations revealed favorable binding at this position to be dominated by hydrogen bond contributions; none of the substitutions (including fluorine) out-performed the native –OH substituent which can act both as hydrogen bond donor and acceptor. The structural analyses of these compounds can be exploited towards the development of better inhibitors.

1. Introduction

Treatment of type 2 diabetes (T2D) has focused mainly on approaches that aim to decrease the high concentration of glucose in the blood by means of hypoglycaemic drugs, such as sulfonylureas that increase the insulin secretion rate of the β-cell islets but also can cause rather significant mechanism-based side effects. The liver is principally responsible for the elevated rates of glucose during the processes of gluconeogenesis and glycogenolysis. Glycogen phosphorylase (GP) a key regulatory enzyme present in most mammals, catalyzes the first step of glycogen degradation to glucose-1-phosphate (Glc-1-P) that is subsequently converted to α-D-glucose.[1] In recent years GP has emerged as a promising target for the design of inhibitors with pharmaceutical applications towards improving glycaemic control in type 2 diabetes.[2–4]

The enzyme exists in two interconvertible forms: the dephosphorylated form, GPb, and the phosphorylated form, GPa. In resting muscle the enzyme exists in the inactive form (GPb), which can be activated either by non-covalent co-operative binding of AMP (or IMP) or by covalent phosphorylation to form GPa. Both forms can exist in a less active T state and a more active R state according to the Monod–Wyman–Changeux model for allosteric proteins.[5] The catalytic site, which includes the essential cofactor pyridoxal-5-phosphate, is buried at the center of the subunit

Abbreviations: GP, glycogen phosphorylase, 1,4-α-D-glucan: orthophosphate α-glucosyltransferase (EC 2.4.1.1); GPb, rabbit muscle glycogen phosphorylase b; GPa, rabbit muscle glycogen phosphorylase a; hlGPa, human liver glycogen phosphorylase a; PLP, pyridoxal 5′-phosphate; glucose, α-D-glucose; Glc-1-P, α-D-glucose 1-phosphate.

* Corresponding author. Tel.: +30 2410 565278; fax: +30 2410 565290.
E-mail address: ddleonidas@bio.uth.gr (D.D. Leonidas).

0968-0896/$ - see front matter © 2010 Elsevier Ltd. All rights reserved.
doi:10.1016/j.bmc.2010.04.004

accessible to the bulk solvent through a 15 Å long channel. The catalytic site of GP has been probed with glucose and glucose analogues inhibitors.[2] Glucose is an effective allosteric inhibitor for GP and it exhibits a Hill coefficient ($n = 1.5$) that indicates a shift in the equilibrium toward the T state.[2] Glucose, on binding at the catalytic site, promotes the less active T state through stabilization of the closed position of the 280s loop which blocks access for the substrate (glycogen) to the catalytic site. The binding of glucose at the catalytic site is dominated by hydrogen bonds from each of the peripheral hydroxyl groups to protein atoms. Examination of the van der Waals surface of α-D-glucose bound to GPb showed that, there is an empty pocket at the β-1-C configuration lined by both polar and non polar groups.[2] A systematic work of structure-assisted design, based on synthetic, kinetic, and X-ray crystallographic binding studies has led to the discovery of over 80 glucose analogues inhibitors of GPb.[2–4] *N*-Acetyl-β-D-glucopyranosylamine (NAG) was one of the first efficient glucose analogue inhibitors of GP[6], and has been used as a lead in inhibitor design.[4] Inhibitors with substituent large aromatic groups or long rigid aliphatic chain with an aromatic endgroup increase the potency.[3,4] Furthermore, the potency and the binding mode of *N*-β-D-glucopyranosylamines, *N*-acyl-*N*′-β-D-glucopyranosyl ureas, glucose analogues based on *C*-β-D-glucopyranosyl derivatives, glucose analogs based on iminosugars, *N*-β-D-glucopyranosyl monoamides of dicarboxylic acids, *N*-β-D-glucopyranosyl oxamic acid and oxamide derivatives, *N*-acyl-*N*′-β-D-glucopyranosylamines to GP has been studied by kinetic and crystallographic methods.[3,4] Structural information available from the crystal structure of the GPb–NAG complex at 1.9 Å resolution[7] showed that NAG (**6**), on binding to GPb, promotes the less active T state enzyme through stabilization of the closed position of 280s loop (residues 282–287) and blocks access of the substrate to the catalytic site. The inhibitor fits tightly into the so-called β-pocket, a side channel from the catalytic site with no access to the bulk solvent.[2] In addition, there is a hydrogen bond between N1 of NAG and carbonyl O of His377, an interaction that since then has been observed in all β-D-glucopyranosylamine analogues of β-D-glucopyranose.[2,3]

Identification of the structural determinants contributing to inhibitor binding modes at the catalytic site should provide a better understanding of the mechanism of inhibition of GP and aid in the design of compounds with improved potency against GP. Fluorinated compounds are currently widely used in the treatment of diseases and the inclusion of a fluorine atom in drug molecules has a strategic value in drug design.[8] The inclusion of a fluorine atom in a compound can have profound effects on drug disposition, in terms of distribution, drug clearance and metabolism.[9] Thus, in continuation of our efforts towards discovering potent inhibitors of GP with a therapeutic potential, we have now studied the effect of fluorine substitution in the glucopyranosyl ring of glucose-based inhibitors with respect to their potency and their binding mode to GPb. Replacement of the hydroxyl groups of glucose at 3′, 4′, or 6′ position by fluorine has resulted in a significant decrease at the inhibitory potency for GP with respect to glucose and 3′, 4′, or 6′ deoxy-fluro-glucose displayed K_i values of 200, 25, and 90 mM, respectively.[10,11] Fluorine is a poorer hydrogen bond acceptor than oxygen (it cannot act as a donor)[12] and it affects the hydrogen bonding interactions between the ligand and residues of the catalytic site of GPb that can donate a proton. Moreover, *N*-β-D-glucopyranosyl pyrimidines have been recently found to inhibit GP with K_i values in the micromolar region.[4] With the scope to study whether an *N*-β-D-glucopyranosyl pyrimidine substitution and its interactions within the β-pocket can counteract the decrease of the inhibitory potency of glucose caused by the substitution the 3′ hydroxyl group by fluorine, we report here on the kinetic and crystallographic experiments of five deoxy-fluro-glucose derivatives (**1**–**5**, Scheme 1) with glycogen phosphorylase b. These inhibitors have fluorine instead of hydroxyl at the 3′ position of the glucose moiety and either a uracil (**U**, **1**), or a N^4-benzoyl cytosine (**2**), or a cytosine (**C**, **3**), or a 5-fluorouracil (**5-F-U**, **4**) attached at the 1′ position of the glucopyranose.[13,14] We have also tested the inhibitory potential of 2-deoxy 3-fluoroglucopyranose with a N^4-benzoyl cytosine (**5**) attached at the 1′ position. The best of these inhibitors displays a K_i value of 46 μM. To elucidate the mechanism of inhibition for these compounds (**1**–**5**), the crystal structures of GPb in complex with each one of these inhibitors were determined and refined at high resolution (1.86–2.0 Å). The structures demonstrated that the inhibitors bind preferentially at the catalytic site and promote the less active T state conformation of the enzyme by making several favorable contacts with residues of the 280s loop.

Ligand tautomeric states are still often incorrectly disregarded in computer aided drug design.[3,15–17] Recently, we have highlighted the importance of consideration of ligand ionization/tautomeric states in the GPb binding studies for a set of β-D-glucose pyrimidine derivatives.[3] In this respect, we have also calculated using DFT and docked using GLIDE[18,19] the low-lying energy tautomers of **2** and **5**. With respect to ligands **1**, **3**, and **4**, computational studies on the unbound and GPb bound states of β-D-glucose forms of these ligands are reported in our previous work,[3] and are consistent with the crystallographic data reported here for their F-substituted glucose forms, binding through their most state free state tautomeric forms. Finally, to further analyze the binding details of 3′-fluorinated glucose and the potential of a series of other 3′ glucose substitutions (**7_R═X**, Fig. 5), supplementary molecular modelling calculations were performed. The α-D-glucose ligand with a $K_i = 1.7$ mM for GPb inhibition[2] and the reported GPb–α-D-glucose X-ray complex by Martin et al.[20] were used as a template and benchmark. Effects, if any, of substitution on the glucose ring conformations in the free states were monitored, while Glide and quantum mechanics polarized ligand docking (QPLD) calculations[19] were used to model the ligand GPb bound states and properties.

2. Results and discussion

The kinetic parameters of compounds **1**–**5**, assayed with GPb in the direction of glycogen synthesis, are summarized in Scheme 1. Compound **2** was found to be the best inhibitor (on the μM scale ($K_i = 46.42 \pm 1.56$ μM) with the other ligands displaying mM range inhibition (K_i's = 3.46 ± 0.07 mM (**1**); 4.01 ± 0.05 mM (**3**); 3.67 ± 0.30 mM (**4**); 6.55 ± 0.68 mM (**5**)). In order to elucidate the structural basis of inhibition we have determined the crystal structures of GPb in complex with each of **1**–**5**. A summary of the data processing and refinement statistics for the **1**–**5** complex structures is given in Table 1. The initial σ*A* weighted $F_o - F_c$ Fourier electron density maps calculated with phases from the GPb model indicated that compounds **1**–**5** are all bound at the catalytic site (Fig. 1). Electron density maps (Supplementary Fig. 1) clearly defined the position of each inhibitor within the catalytic site, consistent with the kinetic results. A structural comparison between GPb–**2** complex and **1**, **3**, **4**, and **5** GPb complexes shows that the positions of Ca for residues 18–249, 262–312, and 326–829 deviate from their mean positions by 0.083, 0.108, 0.071, and 0.144 Å, respectively, indicating overall negligible changes between the complex structures. The solvent accessibilities of the free ligand molecules **1**–**5** are 424, 579, 432, 446, and 571 Å^2, respectively, while for the bound ligand molecules are 22, 21, 24, 22, and 27 Å^2, respectively. These values indicate that approximately 95% of the surface of all ligands becomes buried upon binding to GP. We describe in detail the GPb–**2** interactions and briefly the interactions of **1**, **3**, **4**, and **5** at the catalytic site.

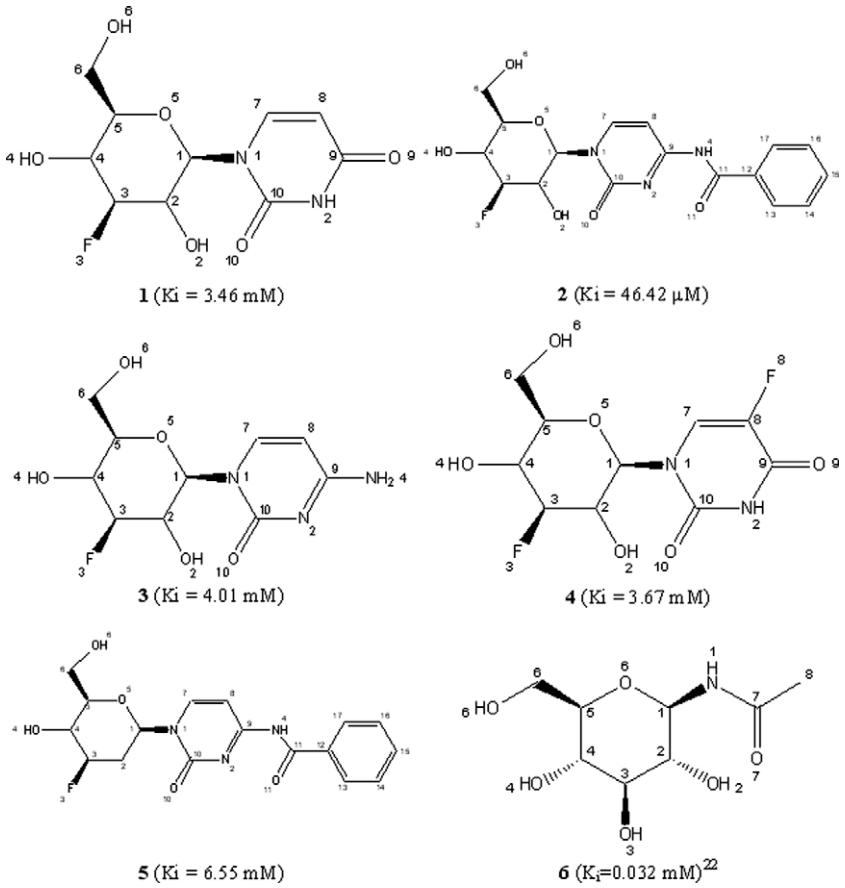

Scheme 1. The chemical structures of the deoxy-fluro-glucose derivatives (**1**–**5**) and *N*-acetyl-β-D-glucopyranosylamine (**6**). The numbering scheme used is shown together with the K_i values for each inhibitor.

Table 1
Summary of the diffraction data processing and refinement statistics for GPb: **1**–**5** complexes

Compound	**1**	**2**	**3**	**4**	**5**
Experimental details					
Inhibitor concentration (mM)	10	10	50	10	50
Soaking time (h)	14	1	5.5	9	48
Resolution (Å)	30.0–1.86	30.0–1.90	30.0–2.0	30.0–1.93	30.0–2.0
Outermost shell (Å)	1.89–1.86	1.93–1.90	2.03–2.0	1.96–1.93	2.03–2.0
Reflections measured	623,051	586,292	943,593	614,856	300,097
Unique reflections	81,842	76,656	66,468	74,225	65,585
Redundancy	5.0 (4.7)	5.0 (5.1)	5.1 (5.3)	4.8 (4.4)	5.0 (4.8)
R_{symm}[a]	0.041 (0.420)	0.044 (0.444)	0.071 (0.487)	0.047 (0.425)	0.051 (0.493)
Completeness (%)	99.4 (99.8)	98.7 (99.9)	99.2 (98.8)	99.9 (99.9)	97.5 (98.3)
$\langle I/\sigma I \rangle$	20.2 (3.8)	19.1 (4.1)	9.4 (5.1)	20.8 (4.2)	4.9 (2.2)
R_{cryst}[b]	0.182 (0.241)	0.182 (0.231)	0.188 (0.235)	0.175 (0.226)	0.184 (0.243)
R_{free}[c]	0.208 (0.302)	0.211 (0.281)	0.215 (0.244)	0.207 (0.255)	0.215 (0.281)
No of solvent molecules	375	348	277	388	295
RMSD from ideality					
in bond lengths (Å)	0.009	0.009	0.010	0.009	0.010
in angles (°)	1.1	1.1	1.2	1.1	1.2
Average B factor					
Protein atoms (Å^2)	29.2	29.2	32.7	27.1	30.8
Solvent molecules (Å^2)	39.1	38.4	39.0	37.6	38.0
Ligand atoms (Å^2)	26.1	38.0	28.4	33.8	28.8
PDB code					

[a] $R_{symm} = \Sigma_h \Sigma_i |I(h) - I_i(h)| / \Sigma_h \Sigma_i I_i(h)$ where $I_i(h)$ and $I(h)$ are the *i*th and the mean measurements of the intensity of reflection *h*.
[b] $R_{cryst} = \Sigma_h |F_o - F_c| / \Sigma_h F_o$, where F_o and F_c are the observed and calculated structure factors amplitudes of reflection *h*, respectively.
[c] R_{free} is equal to R_{cryst} for a randomly selected 5% subset of reflections not used in the refinement. Values in parentheses are for the outermost shell.

2.1. The binding of compound 2 to GPb

The mode of binding and the interactions that the glucopyranose moiety of **2** makes with GPb are close to those for α-D-glucose[21] (Fig. 2). The 3′ fluorine forms hydrogen bonds with the main-chain amide of Ala673, Ser674, and Gly675. In the GPb–NAG complex[7] the glucose moiety forms similar hydrogen bond interactions with the protein residues with the exception of the

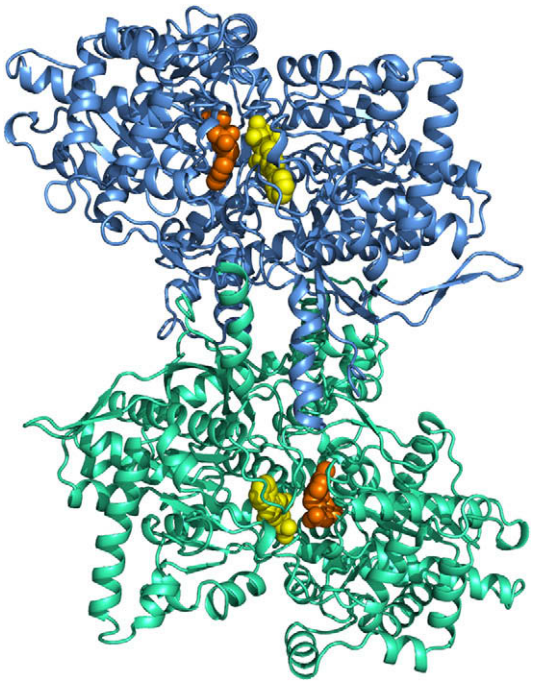

Figure 1. A schematic diagram of the GPb dimeric molecule viewed down the molecular dyad. One subunit is colored in green and the other in cyan. The position is shown for the catalytic site. The catalytic site, marked by bound compound **2** (in yellow), and the essential cofactor pyridoxal 5′-phosphate (in brown) shown in ball-and-stick representations, is buried at the center of the subunit and is accessible to the bulk solvent through a 15-Å long channel. Compound **2**, on binding at the catalytic site, promotes the less active T state through stabilization of the closed position of the 280s loop (shown in red and thicker) which blocks access for the substrate (glycogen) to the catalytic site.

interaction with the main-chain nitrogen of Ala673 which is missing. The N^4-benzoyl cytosine group of compound **2** is accommodated at the β-pocket of the catalytic site stabilizing the closed conformation of the 280s loop. O10 makes a hydrogen bonding interactions with Asn284 Nδ2 and with Asp283 Oδ1 through a water molecule with N2 forming a water-mediated hydrogen bond with Asp283 Oδ1. Compound **2** also exploits an extended hydrogen bonding pattern between N4, a water molecule and Glu88 OE2 and Asn282 O; O10 a water molecule and Gly135 N, and Arg5697 N through another water molecule; O2 is hydrogen bonded with Thr671 O and Ala673 N through a water molecule; O4 forms water-mediated hydrogen bond interactions with Thr676 N and OG1; O6 is hydrogen bonded with His377 ND2 and Asn484 OD1 (Table 2). The hydrogen bonds formed between the ligand and the protein are illustrated in Figure 3b. Compound **2**, on binding to GPb, makes a total of 17 hydrogen bonds and 55 van der Waals interactions with 12 protein residues (1 non polar/non polar, 32 non polar/polar, and 21 polar/non polar) (Table 3). It is a moderate inhibitor (K_i = 46.4 μM) and binds almost as tight as NAG (K_i = 32 μM).[22] However, compound **2** binds 37 times more tightly than α-D-glucose (K_i = 1.7 mM)[2], and 160 times more tightly than its parent compound β-D-glucose (K_i = 7.4 mM)[21] despite the fact that has a fluorine instead of a hydroxyl group at 3′ position which leads to an increase of 100 times in the K_i value of 3-fluoro-3-deoxy-D-glucose with respect to glucose.[10] This can be attributed to the hydrogen bond and van der Waals interactions of the N^4-benzoyl cytosine group with the protein at the β-pocket.

Compound **2** is more bulky than NAG and it was expected to form an improved network of interactions compared to NAG[22], however, it exhibits approximately the same affinity. Structural comparison of the two complexes (Fig. 2) reveals a conformational shift for Asp339; the dihedral angle χ^2 [CA-CB-CG-OD1] is rotated by 90° in order to avoid close contacts with benzoyl group of **2**. There are also small shifts of the side chain atoms of Leu136 and Asp283; thus, on ligand binding, the side chains of Leu136 and Asp283 are rotated by ~90° and 12°, respectively (dihedral angles χ^2 (CA-CB-CG-CD1) and χ^2 (CA-CB-CG-OD1)) to optimize contacts with the ligand. In the GPb–NAG complex, O7 is hydrogen bonded to a water molecule, and this in turn is hydrogen bonded to Asn284 N, and to Asn133 ND2, Glu88 OE1, and Asn282 O through another water molecule.[22] These two water molecules are displaced by the benzoyl group in the GPb–**2** complex. One of the main differences in the binding mode of the two inhibitors appears to be the hydrogen bond interaction of N1 with His377 O in the GPb–NAG complex which does not exist in the GPb–**2** complex since N1 does not have a hydrogen. Ligand **2** also engages in more than double van der Waals interactions (54) than NAG (25)[7] which counteract for the weaker hydrogen bonding interactions of the fluorine atom of **2** as compared to those of the 3′ hydroxyl of NAG offering a possible explanation for their equipotency.

2.2. The binding of compounds 1, 3, and 4 to GPb

Reduction in the size of the 1-substituent group of compound **2** resulted in reduction in the inhibitory potency. Thus, compounds **1**, **3**, and **4** are approximately equipotent inhibitors of GPb with K_i values of 3.46, 4.01, and 3.67 mM, respectively, binding to the enzyme almost 100 times less tight than compound **2**. The mode of

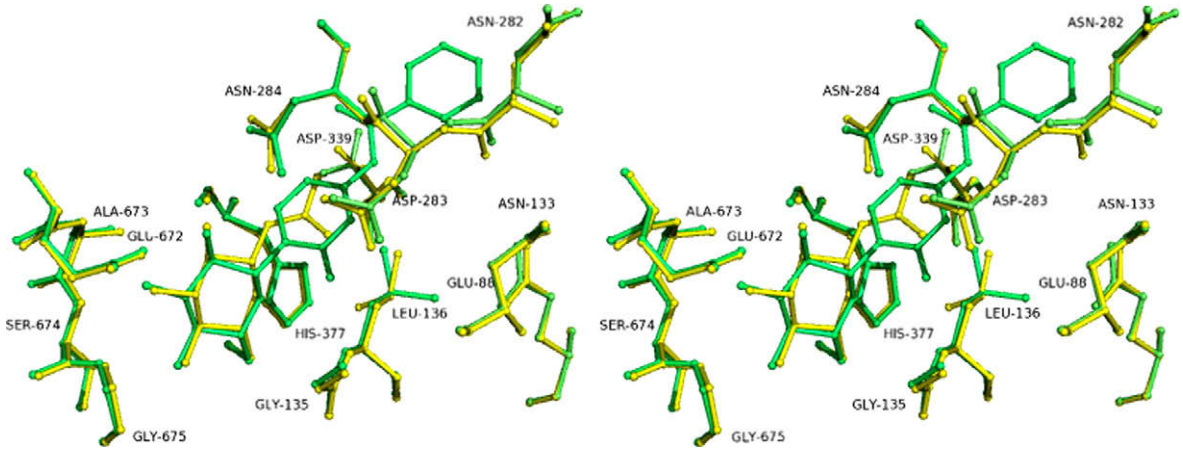

Figure 2. Stereo diagrams of the structural comparison between GPb in complex with **2** (yellow) and NAG (green).

Table 2
Potential hydrogen bond interaction of compounds **1**–**5** with GPb residues in the crystal

Inhibitor atom	GPb–**1**	GPb–**2**	GPb–**3**	GPb–**4**	GPb–**5**
N4		Asn284 N (3.2) Water298 (3.3)			Water266 (3.1)
N2	Water280 (2.6)	Water272 (2.6)	Water240 (2.7)	Water281 (2.4)	Water254 (2.8) Water268 (3.1)
O2	Asn284 Nδ2 (3.2) Tyr573 Oη (3.1) Glu672 Oε1 (2.8) Water285(2.9)	Tyr573 Oη (3.1) Glu672 Oε1 (2.8) Water277 (2.9)	Asn284 Nδ2 (3.3) Tyr573 Oη (3.1) Glu672 Oε1 (2.8) Water242 (3.0)	Asn284 Nδ2 (3.3) Tyr573 Oη (3.1) Glu672 Oε1 (2.8) Water282 (3.2) Water288 (3.0)	
O4	Gly675 N (2.9) Water127 (2.6)	Gly675 N (2.9) Water123 (2.6)	Gly675 N (2.9) Water118 (2.6)	Gly675 N (2.8) Water125 (2.5)	Gly675 N (2.8) Water119 (2.6)
O6	His377 Nδ1 (2.7) Asn484 Oδ1(2.8)	His377 Nδ1 (2.6) Asn484 Oδ1(2.9)	His377 Nδ1 (2.7) Asn484 Oδ1(2.9)	His377 Nδ1 (2.7) Asn484 Oδ1(2.8)	His377 Nδ1 (2.6) Asn484 Oδ1(3.0)
O9	Asn284 N (2.9) Water295 (2.7)			Asn284 N (2.9) Water296 (2.6)	Asn284 Oδ1 (3.3)
O10	Gly135 N (3.3) Leu136 N (3.0) Water58 (3.0) Water280 (3.3)	Gly135 N (3.3) Leu136 N (2.9) Water57 (3.2) Water272 (2.6)	Leu136 N (3.0) Water55 (3.1) Water240 (2.9)	Gly135 N (3.1) Leu136 N (3.0) Asn283 Oδ1(3.3) Water58 (2.8) Water281 (3.1)	Leu136 N (3.0) Water54 (3.1) Water254 (2.7)
F2				Asn284 Oδ1 (3.3) Water296 (3.2)	
F3	Ala673 N (3.3) Ser674 N (2.9) Gly675 N (3.1)	Ala673 N (3.2) Ser674 N (2.9) Gly675 N (3.1)	Ala673 N (3.3) Ser674 N (2.9) Gly675 N (3.1)	Ala673 N (3.2) Ser674 N (2.9) Gly675 N (3.1)	Ala673 N (3.2) Ser674 N (2.9) Gly675 N (3.2)

For ligand atom definitions see Scheme 1. Values in parentheses are distances in Å.

binding and the interactions that the glucopyranose moiety of **1**, **3**, and **4** make with GPb residues are almost identical with those for α-D-glucose[21] and very similar with each other. Fluorine in all three compounds forms hydrogen bonds with the main-chain amides of Ala673, Ser674, and Gly675 as in compound **2**. The 1-substituent group is accommodated at the β-pocket of the catalytic site and stabilizes the closed conformation of the 280s loop. However, its interactions are fewer than compound's **2** and overall compounds **1**, **3**, and **4** form 35, 34, and 37 van der Waals contacts with GPb residues, respectively (Table 3). In particular, compound **1** forms 18 non polar/polar and 16 non polar/non polar, compound **3** 17 non polar/polar, and 15 non polar/non polar, and compound **4** 21 non polar/polar and 14 non polar/non polar van der Waals interactions (Table 3). The pattern of hydrogen bonding interactions, illustrated in Figure 3a–d, between the inhibitors and the enzyme is maintained when comparing the complex structures of derivatives **1**, **3**, and **4**. It is notable that, as in the case of compound **2**, exactly the same conformational rearrangements are observed on binding of **1**, **3**, and **4** to the catalytic site of GPb. These include small shifts in the side chains of Leu136, Asn282, Asp283, Asn284, Asp339, and Thr378 in order to optimize contacts with ligands. However, the amide group of cytosine in compound **3** does not form any hydrogen bond interactions with the protein in contrast to the carbonyl of uracil in compounds **1** and **4** which is in hydrogen bonding distance from Asn284 N (Table 2). This is due to a difference in the binding mode of compound **3** with respect to that of **1** and **4**, that is, the pyrimidine ring of **3** is slightly tilted with respect to its position in **1** and **4** (the difference in the angle C2–C1–N1 between **1** and **4** is 4°). In addition the fluorine atom of the fluorouracil group of compound **4** forms hydrogen bonds with Asn284 OD1 and with His341 NE2 through a water molecule (Table 2, Fig. 3). Still, these differences in the interactions of compounds **1**, **3**, and **4** are not translated into differences in the affinity of compounds for GPb and they are equipotent.

The crystal structure of GPb in complex with 1-D-glucopyranosyl uracil and 1-D-glucopyranosyl cytosine has been reported (PDB codes 3BCS and 3DB8, respectively).[3] These ligands are similar to compounds **1** and **3** with the only difference that they have a hydroxyl group at the 3′ position instead of fluorine. Structural comparison between the GPb complexes with **1** and 1-D-glucopyranosyl uracil and **3** and 1-D-glucopyranosyl cytosine reveals that regardless the fluorine atom the ligands bind almost identical to glycogen phosphorylase. However, their inhibitory potencies differ quite substantially since the K_i values for 1-D-glucopyranosyl uracil and 1-D-glucopyranosyl cytosine are 6.1 and 7.7 μM, respectively[3] while for **1** and **3** are 3.46 and 4.01 mM, respectively. This indicates that the fluorine substitution has a profound effect on the potency of the ligands. This can be attributed to two reasons: (1) the 3′ hydroxyl group of the glucose moiety of the ligands forms a hydrogen bond with the side chain of Glu672 a hydrogen bond which cannot be formed with the fluorine since the latter cannot act as donor in hydrogen bond interactions and (2) the greater electronegativity and lower polarisability of fluorine over oxygen, suppresses its electrostatic influence and renders it a poorer hydrogen bond acceptor.[12]

2.3. The binding of compound 5 to GPb

The absence of a polar group at the 2′ position of the β-D-glucopyranose ring has a dramatic effect on the potency. Thus compound **5** whose only difference from **2** is the 2′ hydroxyl group of the glucose moiety binds 140 times less tight than compound **2** and has a K_i = 6.55 mM. With the exception of the interactions of the 2′ hydroxyl group the rest of the hydrogen bond interactions of compound **5** are similar to those of compound **2**. Upon binding compound **5** forms a total 43 van der Waals contacts with 15 residues (23 non polar/polar, and 20 non polar/non polar). The structural comparison of the GPb–**2** complex and the GPb–**5** complex reveals that there is a significant conformational change in the 280s loop (residues 281–287). Thus, this loop in the GPb–**5** complex is displaced by its position in the GPb–**2** complex by approximately 1 Å at the positions of the Cα atoms. The largest difference is for Asp283 (1.18 Å) and the smallest for Phe286 (0.44 Å). This is probably due to the different conformation of the benzoyl group in the two compounds. The plane of the benzoyl ring is rotated by 60° around the bond C11–C12 in **5** from its position in compound **2**. As

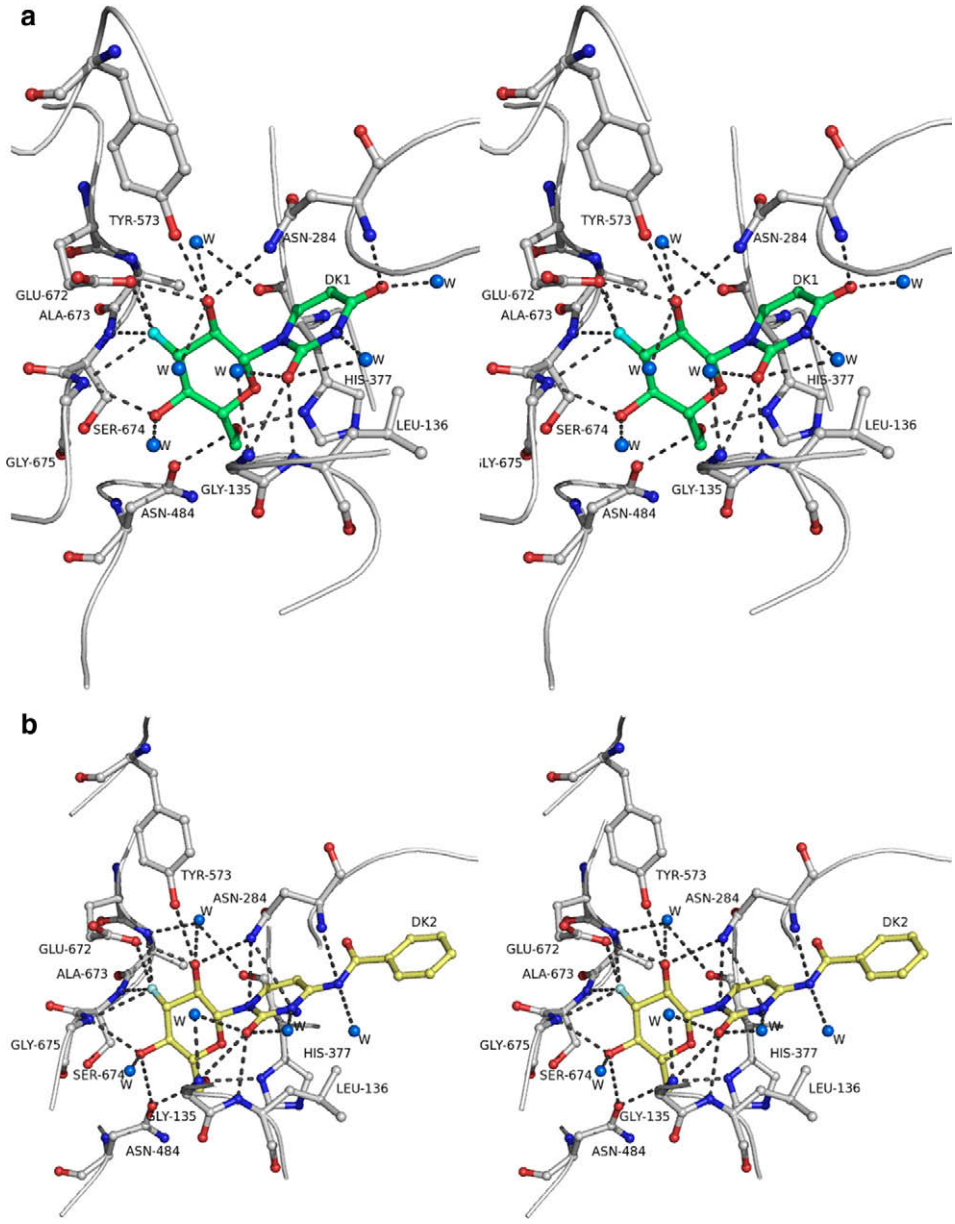

Figure 3. Stereo diagrams of the interactions between GPb and inhibitors **1–5** (a–e). The side chains of protein residues involved in ligand binding are shown as ball-and-stick models. Hydrogen bond interactions between the inhibitors, protein residues, and water molecules (w) are represented as dotted lines.

a result the loop moves away to avoid any steric clashes with the benzoyl atoms of the compound **5**. This conformational change might have an energetic cost, in addition to the loss of the hydrogen bonding interactions of the polar group in position 3′ of glucopyranose, which can explain the lower affinity of compound **5**.

2.4. Modeling

2.4.1. Free state ligand results

2.4.1.1. Compounds 1–5. As mentioned in the introduction, very recently we have investigated a set of β-D-glucose pyrimidine derivatives as GPb catalytic site inhibitors.[3] Included in this set were **U**, **C** and **5-F-U** derivatives, as for our F-substituted glucose ligands **1**, **3**, and **4**, respectively. The free state calculations on the uracil derivative tautomers (**U**, **5-F-U**)[4] revealed the most stable state tautomer (Scheme 1) to be at least ~11 kcal/mol and ~8.5 kcal/mol more stable than other tautomers in gas and solution phases, respectively, using medium level B3LYP and MP2 calculations (water solvation effects were also included using the Poisson–Boltzmann PBF model[23,24]). Further, the **5-F-U** derivative had an estimated pK_a (7.5–8.1) implying partial ionization of its ligand at pH ~7, but binding of the anionic form was not predicted as favorable. All β-D-glucose derivatives of **U**, **C** and **5-F-U** were predicted to bind through their ground state tautomers. Our crystallographic data for the F-substituted glucose form of these ligands (vide supra) is consistent with these predictions.

The tautomeric forms of the **2** and **5** pyrimidine derivatives, meanwhile, required analysis. In our previous work[3], computationally more efficient DFT B3LYP calculations of tautomeric state stabilities were consistent with more expensive MP2 calculations. Also, the 6-31+G* basis set yielded similar relative energies to the much larger aug-cc-PVTZ basis set, particularly in the case of the low energy tautomers. Shown in Figure 6 are the tautomeric relative energies calculated at the B3LYP/6-31+G* level.[25–30] *E* and *Z* conformations, as described in Figure 6, were considered for each tautomer. With **2** and **5** having the same pyrimidine

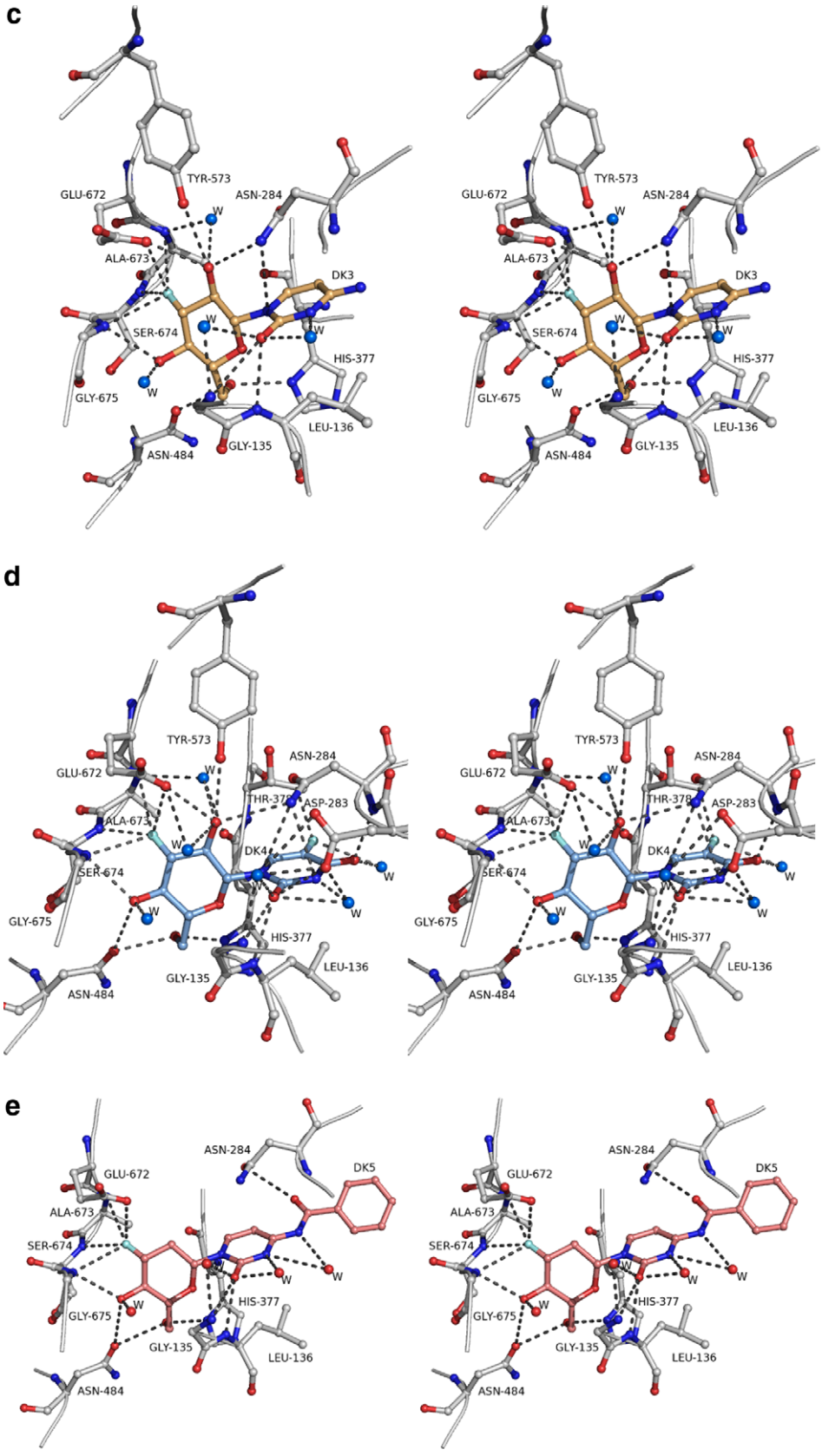

Fig. 3 (*continued*)

derivatives, replacing the glucose moieties with methyl groups simplified and allowed combined analysis of **2** and **5** model tautomers.

There is some difference in the energetic ordering of the tautomers between gas and solution phases; tautomers are listed in order of increasing solution (water) phase energies in Figure 6. In

Table 3
Potential van der Waals interactions of compounds **1–5** with GPb residues upon binding to the catalytic site

Inhibitor atom	GPb–**1**	GPb–**2**	GPb–**3**	GPb–**4**	GPb–**5**
C2	His377 O	His377 O			
C3	Glu672 Oε1; Gly675 N	Glu672 Oε1; Gly675 N	Glu672 Oε1; Gly675 N	Glu672 Oε1; Gly675 N	Glu672 Oε1; Gly675 N
C4		Gly675 N		Gly675 N	
C5	Gly135 Cα, C	Gly135 Cα, C; Leu136 N	Gly135 Cα, C	Gly135 Cα, C; Leu136 N	Gly135 Cα, C; Leu136 N
C6	Gly135 C; Leu136 Cα, Leu139 Cδ2, His377 Nδ1, Cε1; Asn484 Oδ1	Gly135 C; Leu136 Cα; His377 Nδ1, Cε1; Asn484 Oδ1	Gly135 C; Leu136 Cα; Leu139 Cδ2; His377 Nδ1, Asn484 Oδ1	Gly136 C; Leu136 Cα; His377 Nδ1; Cε1; Asn484 Oδ1	Gly135 C; Leu136 Cα; His377 Nδ1; Asn484 Oδ1
C7	Asn284 Cγ, Nδ2; His377 Cβ, C, O	Asn284 Cγ, Oδ1, Nδ2; His377 Cβ, C, O	Asn284 Cγ, Oδ1, Nδ2; His377 Cβ, C, O	Asn284 Cγ, Oδ1, Nδ2; His377 Cβ, C, O	His377 C, O, Cβ
C8	Asn284 Cγ, Oδ1, Nδ2; Thr378 Cβ, Cγ2	Asn284 Cγ, Oδ2, Nδ2; His377 Cβ; Thr378 Cγ2	Asn284 Cγ, Oδ1, Nδ2; His377 Cβ; Thr378 Cγ2	Asn284 Cγ, Oδ1, Nδ2; His377 Cβ	Asn284 Cγ, Oδ1; Thr378 Cγ2
C9	Leu136 Cδ1; Asn284 N, Cα, Cγ, Nδ2	Leu136 Cδ1; Asn284 N, Cγ, Nδ2	Leu136 Cδ1; Asn284 Cα, Cγ, Nδ2	Leu136 Cδ1; Asn284 N, Cα, Cγ, Nδ2	Asn284 Cγ
C10	Leu136 N, Cβ; Asn284 Nδ2	Leu136 N, Cβ; Asn284 Nδ2	Leu136 N, Cβ; Asn284 Nδ2	Leu136 N, Cβ; Asn284 Nδ2	Leu136 Cβ
C11		Asn284 N, Cα			Asn284 N, Cα
C12		Asn284 N, Cα			Asn284 N, Cα
C13					Asp283 C; Asn284 N, Cα, C; Phe285 N; Ala383 Cβ
C14		Phe285 C, O; Phe286 Cα, Cβ; Ala383 O			Phe285 N, C; Phe286 N, Cα
C15		Phe285 C, O			
C16		Phe285 O			Asn282 O; His341 Cε1, Nε2
C17		Asn282 O, His341 Cε1			His341 Cε1, Nε2
O4	Gly675 Cα, C	Gly675 Cα, C	Gly675 Cα, C	Gly675 Cα, C	Gly675 Cα, C
O6	His377 Cε1	His377 Cε1	His377 Cε1	His377 Cε1	His377 Cε1
O9	Asn284 Cα			Asn284 Cα	
O10	Leu136 Cβ	Leu136 Cβ	Leu136 Cβ	Gly135 Cα	Leu136 Cβ
O11		Asn284 Cα; Thr378 Cγ2; Ala 383 Cβ			Asn284 Cα; Thr378 Cγ2; Ala383 Cβ
N1		Asn284 Nδ2	Asn284 Nδ2		
N2		Leu136 Cβ	Leu136 Cβ	Asn284 Nδ2	
N4		Asn284 Cα			
F3	Glu672 Oε1	Glu672 Oε1	Glu672 Oε1	Glu672 Oε1	Glu672 Oε1
F8				Thr378 Cγ2	
Total	35 contacts (9 residues)	55 contacts (12 residues)	34 contacts (9 residues)	37 contacts (8 residues)	44 contacts (15 residues)

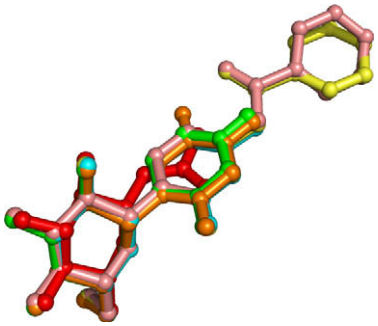

Figure 4. Structural comparisons of the ligand molecules are shown in color; **1** green, **2** yellow, **3** cyan, **4** orange, **5** pink, and NAG red.

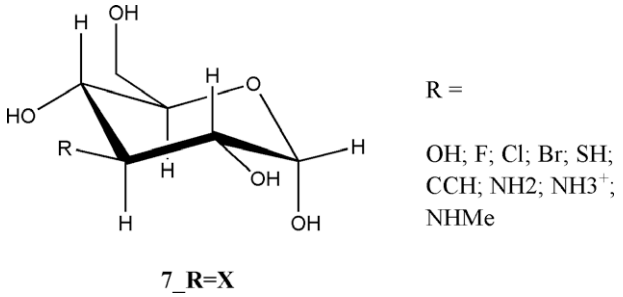

Figure 5. α-D-Glucose with various 3′ position R group substitutions as potential GPb inhibitors studied via computation in this work.

solution, the most stable tautomer (**t**) model (**m**) is **2/5-m-t1-E**, the amide form of the ligand in an *E* conformation. The *E* conformation of **t2** (**2/5-m-t2-E**), the N(3) protonated tautomer, is just 3.6 kcal/mol higher in energy. It is also the *E* forms of **2** and **5** that are bound to GPb in the crystal structures. In the gas phase, however, the *Z* form of **t2** (**2/5-m-t2-Z**) allowing formation of an intramolecular hydrogen bond between N4(H) and the amide carbonyl O is the most favored by about 2 kcal/mol over the preferred solution phase structure (**2/5-m-t1-E**). Hence, while a more extended form of the ligand is preferred in solution, in the gas phase structures with more favorable intramolecular contacts are preferred. The energy differences between tautomer models **t1** and **t2** are small. Shown in Figure 7 are the highest occupied (HOMO) and lowest unoccupied (LUMO) molecular orbitals of **2/5-m-t1-E**. Using a Frontier orbital approach, the HOMO with mainly σ-bonding character and a large magnitude above and below N4, highlights the affinity for H^+ migration from N5 to form **2/5-m-t2-E**. Further, the stability of tautomers/conformations seems to be related to the 'amide' torsion angles τ1–τ4 presented in Figure 6, with more planar conformations (values close to 0° or 180°) favored.

Based on the free state model calculations, the low-lying pyrimidine derivative tautomers (within ~5 kcal/mol of each other) **2/5-m-t1-E**, **2/5-m-t1-Z**, **2/5-m-t2-E** and **2/5-m-t2-Z** were isolated as potential **2** and **5** ligand binding states at the GPb catalytic site; tautomers/conformations of **2** and **5** based on these models were used as input for the docking calculations.

2.4.1.2. 7_R=X ligands (3′-substituted α-D-glucose). For the **7_R=X** ligands, as we were altering the basic properties of the

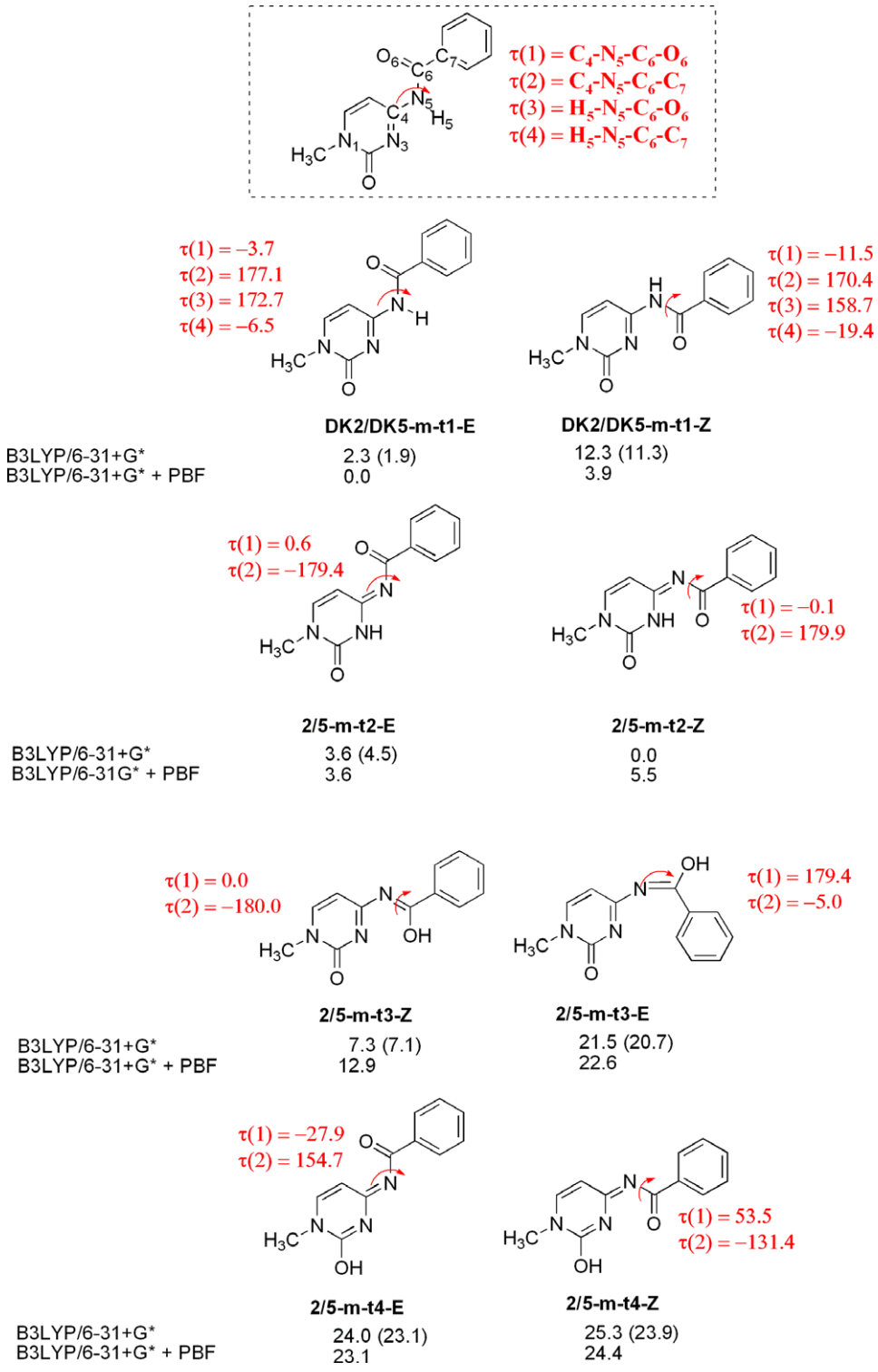

Figure 6. Tautomeric models of compounds **2** and **5** and their relative energies calculated in gas (B3LYP/6-31+G*) and solution (B3LYP/6-31+G* + PBF) phases as described in text, performed to identify the low energy tautomers. For B3LYP/6-31+G*, also shown in parentheses are the gas phase Gibbs energies at 298.15 K. *E* (*trans*) and *Z* (*cis*) conformations of each tautomer were used with respect to the C4–N5 bond: a *Z* conformation in which O6 is close ('*cis*') to the uracil ring N4; and an *E* conformations in which it points away ('*trans*'). The dihedral angles τ(1)–τ(4) around the N5–C6 'amide' bond for the B3LYP/6-31+G* optimized structures are also shown.

glucose moiety through the **R** substitutions, it was important to check that the preferred unsubstituted α-D-glucose conformation, an 'equatorial-rich chair', would remain intact. Conformational searches for eight of the nine **7_R═X** ligands revealed no change in ring conformation. However, in the case of **7_R═CCH**, the conformational searches revealed 'equatorial-rich' and 'axial rich' glucose conformations as the most stable for the MMFFS[31] and OPLS-AA (2005)[32] force fields, respectively. The 'equatorial-rich' conformation was confirmed via DFT optimizations of both conformations, 2.4 kcal/mol and 2.7 kcal/mol more stable in gas (B3LYP/6-31G*) and solution (B3LYP/6-31G*+PBF) phases at the levels of theory used[23–30], respectively.

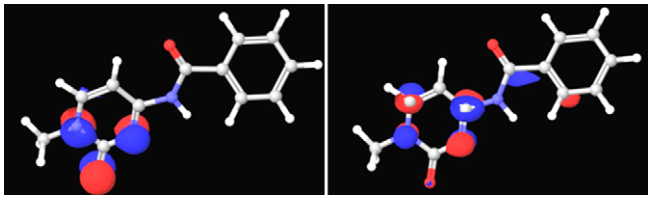

Figure 7. Highest occupied (HOMO; left) and lowest unoccupied (LUMO; right) molecular orbitals of **2/5-m-t1-E** for the B3LYP/6-31+G* optimized structures.

2.4.2. Docking and QM/MM results

2.4.2.1. 2 and 5 binding. To probe the favorable binding states of ligands **2** and **5**, Glide-XP[18,19,33] native receptor docking calculations of the low-lying ligand tautomers/conformations (based on the free state calculations) were performed. Using the top-ranked docking poses, QM/MM calculations were used to determine relative complex energies for the tautomeric complexes, as well as the binding energies ΔE_{bind}. The results of the docking and QM/MM calculations are shown in Table 4. For the Glide-XP docking, compound **2** was predicted to have a much better binding affinity than **5** as judged by the docking GlideScores, consistent with the kinetics results and highlighting the importance of the 2′-OH glucose substituent. RMSDs between the top-ranked Glide-XP poses of each ligand tautomer (*E* conformation) and their crystallographic conformations were in all cases approximately ⩽0.3 Å (Table S1) but due to the small differences for different tautomers cannot be used to distinguish the favored ligand binding form.[3]

Tautomers for compounds **2** and **5** were initially scored in their crystallographic *E* conformation positions ('score-in-place'), using the Glide-SP scoring function[33], with scores for tautomer **2** in both cases (**2-t2** and **5-t2**) slightly better (∼0.2 GS units). For compound **5**, Glide-XP docking convincingly predicted tautomer **1** (**5-t1**) binding with scores at least 1.5 GS units better than tautomer **2**. However, Glide-XP in 'retain' amide conformation mode, incorrectly predicted binding of tautomer **1** in a *Z* conformation. The QM/M results also supported the binding of **5** through tautomer **1**, with the GPb–**5-t1** complex energy 46.1 kcal/mol more stable and ΔE_{bind} = −88.1 kcal/mol compared to −45.8 kcal/mol for **5-t2** at the level of theory/approximations used. The larger than expected energies can be associated mainly with the rigid receptor approximation used; however, use of the crystal structure conformation allowed us to calculate which tautomer/conformation fit best to the experimental receptor structure. For compound **2** docking, the Glide-XP results are conflicting depending on whether amide non-planar conformations are 'penalized' or the 'retain' amide conformation option is used in the Glide-XP docking. When penalize is used, **2-t2** binding in *E* conformation is predicted (GS = −12.91) and **2-t1** can only bind in its *Z* conformation, which is not the crystallographic conformation. However, in 'retain' amide docking mode, the *E* conformation of tautomer **1** is preferred (**2-t1**). The QM/MM results served to resolve the discrepancy, and revealed the GPb–**2-t2** optimized complex to be 20.6 kcal/mol more stable and ΔE_{bind} = −75.6 kcal/mol compared to −52.3 kcal/mol for **5-t1**.

Table 5
Top-ranked docking GlideScores (GSs) for 3′(equatorial)-substituted glucose derivatives using Glide-XP and QPLD(SP-XP) methods. None of the substitutions were predicted to improve ligand binding affinity towards GPb inhibition

Glucose 3′ Substituent	With (without) ligand geometric constraints[a]	
	Glide-XP	QPLD(SP–XP)
–OH	−9.66 (−9.95)	−9.25 (−9.92)
–F	−7.81 (*−6.92**)	−7.78 (−7.97)
–Cl	−7.40 (−8.48)	−7.84 (−8.20)
–Br	−7.58 (−8.01)	−8.20 (−8.57)
–SH	−6.78 (*−6.42**)	−7.69 (−8.70)
–CCH	NP (*−6.45**)	NP (−6.76)
$-NH_2$	−8.31 (−8.93)	−8.73 (−9.83)
$-NH_3^+$	−7.69 (*−9.05**)	*−8.69** (*−9.54**)

[a] GlideScores from docking without glucose ring positional constraints are given in parentheses ( ). Ligand poses which differ from the native glucose (–OH substituent) orientation in the PDB: 2GPB X-ray structure are highlighted in italics and by an asterisk *.

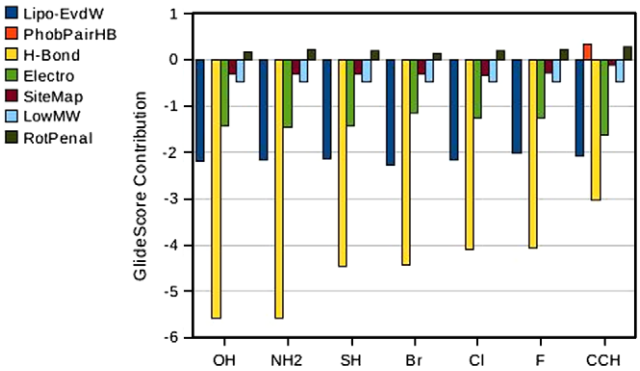

	OH	NH2	SH	Br	Cl	F	CCH
Lipo-EvdW	-2.2	-2.16	-2.13	-2.27	-2.16	-2.04	-2.09
PhobPairHB	0	0	0	0	0	0	0.33
H-Bond	-5.6	-5.59	-4.48	-4.45	-4.11	-4.08	-3.03
Electro	-1.45	-1.48	-1.44	-1.15	-1.27	-1.26	-1.63
SiteMap	-0.31	-0.32	-0.33	-0.32	-0.34	-0.29	-0.11
LowMW	-0.5	-0.5	-0.5	-0.5	-0.5	-0.5	-0.5
RotPenal	0.15	0.21	0.18	0.13	0.18	0.2	0.27
GScore	**-9.92**	**-9.83**	**-8.7**	**-8.57**	**-8.2**	**-7.97**	**-6.76**

Figure 8. Breakdown of the QPLD(SP–XP) docking GlideScores (GSs) into their individual XP term contributions for docking of α-D-glucose derivatives **7_R=X** with different 3′ equatorial substituents (cf. Fig. 5). Clear from the plot is that binding is dominated by the hydrogen bond contributions.

The predicted binding of **2** in its **2-t2** form and **5** in **5-t1** form is consistent with the GPb conformations in the co-crystallized complexes. In the **2**–GPb complex, the carboxylate of the side chain of D283 points towards the ligand where it can form a hydrogen bond with N4(H) of **2-t2**, while in the GPb–**5** complex, the D283 carboxylate points away from the unprotonated form of N4 (**5-t2**) and the ligand carbonyl O reducing repulsive effects.

Table 4
Results of the Glide-XP native docking calculations for ligands **2** and **5**, and the subsequent QM/MM calculations using the top-ranked (*E* conformation) docking poses as described in text

Ligand	Tautomer	Glide docking method (top-ranked pose GlideScore)			QM/MM energies (kcal/mol)	
		SP (score-in-place)	XP (penalize)	XP (retain)	Relative complex energies	ΔE_{bind}
2	**2-t1**	−10.33	−11.98 (*Z*)	−12.40 (*E*)	20.6	−52.3
	2-t2	−10.56	−12.91 (*E*)	−11.67 (*E*)	0.0	−75.6
5	**5-t1**	−9.38	−10.62 (*E*)	−10.77 (*Z*)	0.0	−88.1
	5-t2	−9.54	−8.65 (*E*)	−9.21 (*E*)	46.1	−45.8

2.4.2.2. 7_R=X ligands. On comparing the Glide-XP and QPLD (SP–XP) top-ranked α-D-glucose ligand docking poses with the ligand's crystallographic conformation on redocking to its native receptor (PDB ID: 2GPB), the RMSD (heavy atoms) were only ⩽0.2 Å for in-place comparisons and ⩽0.1 Å after superimposition (Table S2), a preliminary validation of the docking methods used. The Glide docking algorithm and scoring function was previously shown to accurately reproduce the finer details of β-D-glucose moiety binding at the GPb catalytic site.[34] The results of the docking calculations for the **7_R=X** ligands, where **X** represents the different 3′ substituents (equatorial position), are shown in Table 5 and Figure 8. The key result, consistently reproduced by each method, is that none of the 3′-substitutions for –OH in α-D-glucose are predicted to improve the binding affinity. The docking without constraints (cf. Materials and methods) generally led to better docking scores and although the glucose rings of each ligand retain their free state equatorial rich conformations in the bound state, in a few cases mainly for Glide-XP docking, the docking poses do not match the native α-D-glucose orientation in the cavity of the GPb catalytic site (highlighted by an asterisk * in Table 5). For QPLD(SP–XP) docking, only with substituent $-NH_3^+$ does this occur. From Figure 8, it is clear that the dominating term is the hydrogen bonding contribution, all other terms having relatively similar contributions in comparison for the different substituents. The best performer (highest scoring) of the –OH substitutes was **7_R=NH2**, the –NH2 which like OH can act as both a hydrogen bond donor and acceptor. Meanwhile, the –F substituent (**7_R=F**) score is in line with the kinetic results reported above for a counterproductive effect on ligand binding affinities. Its inability to act as both a hydrogen bond donor and acceptor has to be cited in this regard. Of the halide substituents (F, Cl, Br), docking predicted the least electronegative and larger Br atom substitution to be better with respect to favorable hydrogen bonding contributions and overall GPb inhibition.

3. Conclusions

In Figure 4, we compare the binding of **1**–**5** and NAG within the catalytic site of GPb. The positions of the glucosyl components of **1**–**5** are similar, while the largest difference (compared to NAG) is in the amide N1 positions, a difference that might reflect the absence of a hydrogen bond between N1 and main-chain O of His377 in **1**–**5**. In conclusion, five novel 3′-fluorinated derivatives of β-D-glucopyranosylamine, with polar substituents in the amide N1 of the lead compound NAG, were studied for binding at GPb. Compound **2** is the best inhibitor with a K_i similar to that of NAG. All five derivatives form direct and water-mediated hydrogen bonds and extensive van der Waals interactions with residues of the 280s loop (Asp283 and Asn284), the glycine helix (Gly134 and Gly137), Glu88, Asp339, and His341. These interactions provide a rationale for their potency to inhibit GPb activity. In contrast to some previously reported β-D-glucopyranose analogue inhibitors of GP[6,7,35–37] that bind to the catalytic site, compounds **1**–**5** do not exploit the hydrogen bonding interaction between the ligand amide nitrogen and the main-chain carbonyl O of His377 since the amide nitrogen does not have a hydrogen. This interaction is an essential feature for the tight binding of NAG (K_i = 32 μM), contributing approximately 1.1 kcal/mol to the binding energy.[7] The fluorine substitution in the 3′ position of the glucose moiety did not affected the structural mode of binding although it has a substantial effect on the potency since it increased more than 500 times the K_i values of compounds **1** and **3** with respect to NAG. An 100 times increase in the K_i value with respect to that of glucose has been reported for 3-fluoro-3-deoxy-D-glucose.[10] The hydrogen bond of the 3′ glucose hydroxyl with Glu672 OE1, Ser674 N and Gly675 N cannot be formed with fluorine since it cannot act as a hydrogen donor while it is a rather weak hydrogen acceptor. For 3-fluoro-3-deoxy-D-glucose this resulted in a loss of 2.7–3.2 kcal/mol of binding energy[10] and it seems that the same applies for compounds **1**–**5**, although it is more profound for compounds **1**, **3**, **4**, and **5** than for **2**. In the case of compound **2** it seems that the interactions of the N1 substituent group can counteract the loss of the binding energy caused by the replacement of the 3′ hydroxyl in the glycopyranose ring by fluorine.

The present study has demonstrated that the novel analogues **1**–**5** are competitive inhibitors of muscle glycogen phosphorylase albeit with moderate affinity. However, preliminary results with human liver glycogen phosphorylase have shown that compound **2** displays an IC_{50} value of 250 μM. Further work is currently in progress to examine modified analogues with greater potency for the catalytic site of the enzyme.

Binding calculations using docking and QM/MM methods were performed and revealed a preference for the binding of compound **5** through tautomer **5-t1**. In the case of ligand **2**, the QM/MM calculations predicted the slightly higher energy of the **2-t2** tautomer to bind more efficiently to the receptor conformation from the GPb–**2** complex in the crystal. This result was reproduced by Glide-XP docking in 'penalize' non-planar amide mode, but not 'retain' amide conformation mode; ligand model free state calculation results also showed a relation between stabilities and the dihedrals around N5–C6 (planarity of the 'amides'). Binding of compound **2** through **2-t2** and **5** through **5-t1** is consistent with the D283 side chain carboxylate pointing towards and away from the ligands in the GPb–**2** and GPb–**5** crystal structures, respectively. For both **2** and **5**, however, given the calculated small energy differences between their two low energy tautomers, it is likely that the tautomeric forms exist in equilibrium bound at the GPb catalytic site.

Also, we have investigated via docking calculations the potential of different 3′-substitutions (equatorial position) of α-D-glucose for future GPb inhibitor design. None of the substitutions were predicted to improve the potency over α-D-glucose and its native 3′-OH substituent. The binding of the α-D-glucose derivatives is dominated by the ability to form hydrogen bonds which is highly rewarded in the Glide scoring function. The 3′-fluorinated glucose analogue is less favorable in this regard in line with data reported by Howard et al.[12] On this basis, further research on glucose substitutions will retain this –OH, and we are now currently investigating the capabilities of different glucose substitutions in the 3′ axial position, results of which will be reported in due course.

4. Experimental section

4.1. Kinetics

Deoxy-fluoro-glucose derivatives **1**–**5** were synthesized using a method previously described for the synthesis of deoxy-fluoro-glucose pyrimidines.[13,14] Rabbit muscle GPb was isolated, purified, recrystallized, and assayed as described previously.[6] Kinetic experiments were performed in the direction of glycogen synthesis in the presence of constant concentrations of glycogen (0.2% w/v), AMP (1 mM), various concentrations of Glc-1-P (2–20 mM) and inhibitors, in 30 mM imidazole buffer (pH 6.8), 60 mM KCl, 0.6 mM dithiothreitol, 0.6 mM EDTA.[7]

4.2. X-ray crystallography

Structural studies of the protein–inhibitor complexes were performed by diffusing the inhibitors to native T state GPb crystals,

grown as described previously.[6] Soaking conditions are shown in Table 1. X-ray diffraction data for all five inhibitor complexes were collected from single crystals at EMBL-Hamburg outstation (Station X13, $\lambda = 0.81$ Å). Data reduction and integration followed by scaling and merging of the intensities obtained was performed with the HKL suite of programs[38] and intensities were transformed to amplitudes by the program TRUNCATE.[39] Crystallographic refinement of the complexes was performed by maximum-likelihood methods using REFMAC.[40] The starting model employed for the refinement of the complex was the structure of the native T state GPb determined at 1.9 Å resolution (Leonidas et al., unpublished results). Calculated $2F_o - F_c$ and $F_o - F_c$ electron density maps were visualized using the program for molecular graphics COOT.[41] Inhibitor molecules were modelled using the Dundee PRODRG server (http://davapc1.bioch.dundee.ac.uk/programs/prodrg/) and they were included in the refinement procedure during its final stages. Ligand models of compounds **1–5** were fitted to the electron density maps after adjustment of their torsion angles. Alternate cycles of manual rebuilding with COOT and refinement with REFMAC improved the quality of the models. Details of data processing and refinement statistics are provided in Table 1.

The program PROCHECK[42] was used to assess the quality of the final structures. Analysis of the Ramachandran (φ–ψ) plot showed that all residues lie in the allowed regions. Solvent accessible areas were calculated with the program NACCESS.[43] Atomic coordinates and structure factors of the five complexes have been deposited in the Protein Data Bank, (www.pdb.org) with accession numbers 3L79, 3L7A, 3L7B, 3L7C, and 3L7D, respectively. Figures were prepared with the program PYMOL.[44]

4.3. Modelling

4.3.1. Ligand free state calculations

To determine the important (low energy) tautomeric forms/conformations of ligands **2** and **5**, DFT optimizations using the B3LYP[25–27] method and the 6-31+G* basis set[28–30] were performed (B3LYP/6-31+G*). The optimizations were followed by single point energy calculations at the optimum geometries to obtain aqueous solution phase energies using a self-consistent reaction field (SCRF) continuum treatment of solvation which involved accurate numerical solution of the Poisson–Boltzmann (PBF) equation[23,24] (B3LYP/6-31+G* + PBF). For simplicity and speed, the glucose moieties of compounds **2** and **5** were replaced a methyl group. Molecules were prepared using the Schrödinger Maestro and the BUILD module. Two different conformations with respect to the C4–N5 bond for each tautomer were considered (Fig. 6).

Each of the series of 3′-substituted (equatorial position) α-D-glucose ligands **7_R═X** (Fig. 5) were initially prepared using Maestro's BUILD module and LIGPREP (LigPrep, version 2.2). To ensure the **R** substitutions did not disrupt the integrities of the α-D-glucose ring conformations, 1000 steps of the mixed mode Monte Carlo Multiple Minima/Low Mode Conformational Search (MCMM/LMCS) algorithm[45] were performed. Both MMFFS[31] and OPLS-AA (2005)[32] force fields together with the GB/SA continuum model[46] for H_2O solvation effects were used and compared. In cases where conflicting results were obtained for the two force fields, calculations were supplemented by DFT optimizations using the B3LYP/6-31G* method[25–30], followed by single point energy calculations at the optimum geometries including H_2O solvation effects with the PBF method[23,24] (B3LYP/6-31G* + PBF).

For all DFT optimized geometries, frequency calculations were performed to characterize the stationary points as true minima, as well as for calculation of gas-phase Gibbs energies at 298.15 K. All DFT calculations were performed using Jaguar version 7.5[19], while MacroModel version 9.5[19] was used for molecular mechanics/Monte Carlo conformational search calculations.

4.3.2. Ligand docking details

Native docking calculations of ligands **2** and **5** to the receptors prepared from the GPb–**2** and GPb–**5** complexes, respectively, were performed. The low-lying tautomers/conformations of the ligands based on the free state model ligand calculations were minimized (OPLS-AA (2005)[32]; GB/SA for H_2O[46]) and used as input for docking. Meanwhile, docking of the **7R═X** ligands (Fig. 5) was performed using the receptor prepared from the GPb–α-D-glucose complex (PDB ID: 2GPB). Ligand input conformations came from the free state conformational searches as outlined above.

The initial setup of the GPb receptors for docking of the ligands was performed using Schrodingers' 'Protein Preparation Wizard' starting from the Martin et al.[20] GPb–α-D-glucose complex (PDB ID: 2GPB) for **7_R═X** docking, and the GPb–**2** and GPb–**5** crystal complexes for **2** and **5** native docking, respectively. Bond orders were first assigned, hydrogen atoms added and all crystallographic water molecules deleted. The initial assignments of protonation states for basic and acidic residues, and tautomeric states were based on pK_a at their normal pH (7.0). However, subsequent optimization of hydroxyl, histidine protonation states and C/N atom 'flips', and side chain O/N atom 'flips' of Asn and Gln was based on optimizing hydrogen bonding patterns, so that the final assignments were checked on visual inspection of the protein. In particular, all final His residues were assigned as neutral, either in a HIE or HID state. Notably, the His377 was used in a HID state which was further validated by PDB2PQR[47] and PropKa[48,49] calculations on the GPb–α-D-glucose complex. The γ-phosphate in PLP was used in its mono-anion form. Finally, 'Impref' minimizations of the GPb complexes were performed using the OPLS-AA (2005)[32] force field to remove steric clashes and bad contacts. At the end of the minimization, the root–mean–square deviation (RMSD) of all heavy atoms was within 0.3 Å of the crystallographic positions.

Docking calculations were performed using the program GLIDE version 5.0.[18,19,33] The shape and properties of the catalytic binding-site were first mapped onto grids with dimensions of ~19.4 × 19.4 × 19.4 Å centered on the α-D-glucose from the GPb–α-D-glucose complex, and with dimensions ~26.9 × 26.9 × 26.9 Å for the GPb–**2** and GPb–**5** complexes, centered on the ligands **2** and **5**, respectively. Docking calculations were performed in extra-precision (XP) mode with standard vdW scaling (by 0.8) of non polar atoms applied to include modest 'induced fit' effects. Ring conformational sampling was enabled in the docking of **7_R═X** ligands, which was performed with/without 'core' constraints on the six glucose ring atoms. For docking of **2** and **5**, both glucose ring core constraints and positional constraints on glucose O(H) and F atoms were used. Post-docking minimization of the poses was performed with up to three poses per ligand state saved. Ligand poses were considered conformationally distinct if their RMSD (heavy atoms) was larger than 0.5 Å.

Given its effectiveness in our previous studies[3,50], quantum mechanics polarized ligand docking (QPLD) was also performed for the **1R═X** ligands using electrostatic potential (ESP) fit atomic partial charges calculated in the field of the receptor using QSite version 5.0.[19] Initial docking was performed using Glide-SP with the final redocking using the new ESP fit charges in –XP mode (QPLD(SP–XP)). The same general docking conditions (as described above) were used.

4.3.3. QM/MM calculations

Predictions from the Glide-XP native docking of the tautomers of compounds **2** and **5** were supplemented by QM/MM calculations. Gas-phase optimizations of the GPb complexes (receptor frozen) using top-ranked Glide-XP ligand poses (*E* conformations) were followed by single point energy (SPE) calculations at the optimum geometries including water solvation effects (PBF method). The QM regions were chosen as the ligands modelled at the

B3LYP/6-31+G* level of theory[25–30], while the protein was modelled using MM and the OPLS-AA (2005)[32] force field. To calculate ΔE_{bind}, the binding energy of each tautomer, MM (OPLS-AA (2005) + PBF) and QM (B3LYP/6-31+G* + PBF) SPE calculations in solvent[23,24] were also performed for the rigid receptors (crystal structure geometries) and the ligand tautomers, respectively. For the ligand calculations, the free-state tautomeric conformations were taken from B3LYP/6-31+G* optimized geometries of MMFFS force field[31] global minima from MCMM/LMCS (1000 steps; GB/SA for H_2O[46] effects) conformational searches.[45] It should be noted that in this respect, the OPLS-AA (2005) force field did not produce a global minimum conformation for ligand **5** consistent with the DFT model calculation results in Figure 6. The QM, MM and hybrid QM/MM calculations were performed using Jaguar version 7.5, Impact version 5.0) and QSite version 5.0[19], respectively.

Acknowledgements

We would like to thank Mr. C. Georgousakis, for help with the X-ray crystallographic data processing and Drs. D. Papahatjis and M. Koufaki for useful discussions during the writing of this paper. This work was supported by the Commission of the European Communities—under the FP7 'SP4-Capacities Coordination and Support Action, Support Actions' EUROSTRUCT project (CSA-SA_FP7-REGPOT-2008-1 Grant Agreement No. 230146). This work was also supported by grants from European Community-Research Infrastructure Action under the FP6 'Structuring the European Research Area' Programme (through the Integrated Infrastructure Initiative 'Integrating Activity on Synchrotron and Free Electron Laser Science') for work at the Synchrotron Radiation Source MAX-lab, Lund, Sweden, and EMBL-Hamburg Outstation, Germany.

Supplementary data

Supplementary data associated with this article can be found, in the online version, at doi:10.1016/j.bmc.2010.04.004.

References and notes

1. Newgard, C. B.; Hwang, P. K.; Fletterick, R. J. *Crit. Rev. Biochem. Mol. Biol.* **1989**, *24*, 69.
2. Oikonomakos, N. G. *Curr. Protein Pept. Sci.* **2002**, *3*, 561.
3. Somsak, L.; Czifrak, K.; Toth, M.; Bokor, E.; Chrysina, E. D.; Alexacou, K. M.; Hayes, J. M.; Tiraidis, C.; Lazoura, E.; Leonidas, D. D.; Zographos, S. E.; Oikonomakos, N. G. *Curr. Med. Chem.* **2008**, *15*, 2933.
4. Oikonomakos, N. G.; Somsak, L. *Curr. Opin. Invest. Drugs* **2008**, *9*, 379.
5. Monod, J.; Wyman, J.; Changeux, J. P. *J. Mol. Biol.* **1965**, *12*, 88.
6. Oikonomakos, N. G.; Kontou, M.; Zographos, S. E.; Watson, K. A.; Johnson, L. N.; Bichard, C. J. F.; Fleet, G. W. J.; Acharya, K. R. *Protein Sci.* **1995**, *4*, 2469.
7. Anagnostou, E.; Kosmopoulou, M. N.; Chrysina, E. D.; Leonidas, D. D.; Hadjiloi, T.; Tiraidis, C.; Zographos, S. E.; Gyorgydeak, Z.; Somsak, L.; Docsa, T.; Gergely, P.; Kolisis, F. N.; Oikonomakos, N. G. *Bioorg. Med. Chem.* **2006**, *14*, 181.
8. Park, B. K.; Kitteringham, N. R.; O'Neill, P. M. *Annu. Rev. Pharmacol. Toxicol.* **2001**, *41*, 443.
9. Park, B. K.; Kitteringham, N. R. *Drug Metab. Rev.* **1994**, *26*, 605.
10. Street, I. P.; Armstrong, C. R.; Withers, S. G. *Biochemistry* **1986**, *25*, 6021.
11. Sprang, S. R.; Goldsmith, E. J.; Fletterick, R. J.; Withers, S. G.; Madsen, N. B. *Biochemistry* **1982**, *21*, 5364.
12. Howard, J. A. K.; Hoy, V. J.; OHagan, D.; Smith, G. T. *Tetrahedron* **1996**, *52*, 12613.
13. Manta, S.; Agelis, G.; Botic, T.; Cencic, A.; Komiotis, D. *Bioorg. Med. Chem.* **2007**, *15*, 980.
14. Manta, S.; Agelis, G.; Botic, T.; Cencic, A.; Komiotis, D. *Eur. J. Med. Chem.* **2008**, *43*, 420.
15. Pospisil, P.; Ballmer, P.; Scapozza, L.; Folkers, G. *J. Recept. Signal Transduct. Res.* **2003**, *23*, 361.
16. Oellien, F.; Cramer, J.; Beyer, C.; Ihlenfeldt, W. D.; Selzer, P. M. *J. Chem. Inf. Model.* **2006**, *46*, 2342.
17. Todorov, N. P.; Monthoux, P. H.; Alberts, I. L. *J. Chem. Inf. Model.* **2006**, *46*, 1134.
18. Friesner, R. A.; Murphy, R. B.; Repasky, M. P.; Frye, L. L.; Greenwood, J. R.; Halgren, T. A.; Sanschagrin, P. C.; Mainz, D. T. *J. Med. Chem.* **2006**, *49*, 6177.
19. Schrodinger, L. L. C.: New York, 2008.
20. Martin, J. L.; Withers, S. G.; Johnson, L. N. *Biochemistry* **1990**, *29*, 10745.
21. Martin, J. L.; Veluraja, K.; Ross, K.; Johnson, L. N.; Fleet, G. W. J.; Ramsden, N. G.; Bruce, I.; Orchard, M. G.; Oikonomakos, N. G.; Papageorgiou, A. C.; Leonidas, D. D.; Tsitoura, H. S. *Biochemistry (USA)* **1991**, *30*, 10101.
22. Hadjiloi, T.; Tiraidis, C.; Chrysina, E. D.; Leonidas, D. D.; Oikonomakos, N. G.; Tsipos, P.; Gimisis, T. *Bioorg. Med. Chem.* **2006**, *14*, 3872.
23. Tannor, D. J.; Marten, B.; Murphy, R.; Friesner, R. A.; Sitkoff, D.; Nicholls, A.; Ringnalda, M.; Goddard, W. A.; Honig, B. *J. Am. Chem. Soc.* **1994**, *116*, 11875.
24. Marten, B.; Kim, K.; Cortis, C.; Friesner, R. A.; Murphy, R. B.; Ringnalda, M. N.; Sitkoff, D.; Honig, B. *J. Phys. Chem.* **1996**, *100*, 11775.
25. Becke, A. D. *J. Chem. Phys.* **1993**, *98*, 5648.
26. Lee, C. T.; Yang, W. T.; Parr, R. G. *Phys. Rev. B* **1988**, *37*, 785.
27. Stephens, P. J.; Devlin, F. J.; Chabalowski, C. F.; Frisch, M. J. *J. Phys. Chem.* **1994**, *98*, 11623.
28. Hehre, W. J.; Ditchfie, R.; Pople, J. A. *J. Chem. Phys.* **1972**, *56*, 2257.
29. Hariharan, P. C.; Pople, J. A. *Theor. Chim. Acta* **1973**, *28*, 213.
30. Francl, M. M.; Pietro, W. J.; Hehre, W. J.; Binkley, J. S.; Gordon, M. S.; Defrees, D. J.; Pople, J. A. *J. Chem. Phys.* **1982**, *77*, 3654.
31. Halgren, T. A. *J. Comput. Chem.* **1999**, *20*, 730.
32. Kaminski, G. A.; Friesner, R. A.; Tirado-Rives, J.; Jorgensen, W. L. *J. Phys. Chem. B* **2001**, *105*, 6474.
33. Friesner, R. A.; Banks, J. L.; Murphy, R. B.; Halgren, T. A.; Klicic, J. J.; Mainz, D. T.; Repasky, M. P.; Knoll, E. H.; Shelley, M.; Perry, J. K.; Shaw, D. E.; Francis, P.; Shenkin, P. S. *J. Med. Chem.* **2004**, *47*, 1739.
34. Alexacou, K. M.; Hayes, J. M.; Tiraidis, C.; Zographos, S. E.; Leonidas, D. D.; Chrysina, E. D.; Archontis, G.; Oikonomakos, N. G.; Paul, J. V.; Varghese, B.; Loganathan, D. *Proteins* **2008**, *71*, 1307.
35. Watson, K. A.; Mitchell, E. P.; Johnson, L. N.; Gruciani, G.; Son, J. C.; Bichard, C. J. F.; Fleet, G. W. J.; Oikonomakos, N. G.; Kontou, M.; Zographos, S. E. *Acta Crystallogr., Sect. D* **1995**, *51*, 458.
36. Chrysina, E. D.; Oikonomakos, N. G.; Zographos, S. E.; Kosmopoulou, M. N.; Bischler, N.; Leonidas, D. D.; Kovacs, L.; Docsa, T.; Gergely, P.; Somsak, L. *Biocatal. Biotransform.* **2003**, *21*, 233.
37. Watson, K. A.; Chrysina, E. D.; Tsitsanou, K. E.; Zographos, S. E.; Archontis, G.; Fleet, G. W.; Oikonomakos N. G. *Proteins* **2005**, *61*, 966.
38. Otwinowski, Z.; Minor, W.. In *Methods Enzymol.*; Carter, C. W. J., Sweet, R. M., Eds.; Academic Press: New York, 1997; Vol. 276, p 307.
39. French, S.; Wilson, K. S. *Acta Crystallogr., Sect. A* **1978**, *34*, 517.
40. Murshudov, G. N.; Vagin, A. A.; Dodson, E. J. *Acta Crystallogr., Sect. D* **1997**, *53*, 240.
41. Emsley, P.; Cowtan, K. *Acta Crystallogr., Sect. D* **2004**, *60*, 2126.
42. Laskowski, R. A.; MacArthur, M. W.; Moss, D. S.; Thornton, J. M. *J. Appl. Crystallogr.* **1993**, *26*, 283.
43. Hubbard, S. J.; Thornton, J. M. 'NACCESS', Computer Program, Department of Biochemistry and Molecular Biology, University College London, 1993.
44. The PyMOL Molecular Graphics System, Version 1.2r3pre; Schrödinger LLC.
45. Kolossvary, I.; Guida, W. C. *J. Am. Chem. Soc.* **1996**, *118*, 5011.
46. Still, W. C.; Tempczyk, A.; Hawley, R. C.; Hendrickson, T. *J. Am. Chem. Soc.* **1990**, *112*, 6127.
47. Dolinsky, T. J.; Czodrowski, P.; Li, H.; Nielsen, J. E.; Jensen, J. H.; Klebe, G.; Baker, N. A. *Nucleic Acids Res.* **2007**, *35*, W522.
48. Li, H.; Robertson, A. D.; Jensen, J. H. *Proteins* **2005**, *61*, 704.
49. Bas, D. C.; Rogers, D. M.; Jensen, J. H. *Proteins* **2008**, *73*, 765.
50. Benltifa, M.; Hayes, J. M.; Vidal, S.; Gueyrard, D.; Goekjian, P. G.; Praly, J. P.; Kizilis, G.; Tiraidis, C.; Alexacou, K. M.; Chrysina, E. D.; Zographos, S. E.; Leonidas, D. D.; Archontis, G.; Oikonomakos, N. G. *Bioorg. Med. Chem.* **2009**, *17*, 7368.